

# Diamagnetic nature of stratified thin metals in visible range

Masanobu Iwanaga\*

Department of Physics, Graduate School of Science, Tohoku University, Sendai 980-8578, Japan

(Dated: February 9, 2020)

We numerically demonstrate effectively strong diamagnetic resonance at visible frequencies in stratified metal-dielectric metamaterials. The effective optical constants are extracted by two complex reflectivity method. It is clarified that the effective diamagnetic response emerges at effective plasma frequency and originates from mesoscopic stratified layers of thin metals. Consequently, the diamagnetic response is regarded as a collective excitation in mesoscopic scale. In addition, it is shown that the diamagnetic resonance is spatially dispersive and the diamagnetism is sensitive to the surface layer.

PACS numbers: 42.25.Bs, 42.70.Qs, 78.20.Ci, 73.22.Lp

Photonic metamaterials are trials to invent and produce novel electromagnetic (EM) states by modifying periodic structures in which constituents have the same optical constants with bulk materials. The trials start at gigahertz and proceed to terahertz and optical frequencies with remarkable progress reviewed in Refs. [1, 2]. The strategy is mainly based on the control of geometrical structures in metamaterials, is to seek novel effective EM states which are solutions of Maxwell equations for a homogenized system obtained by coarse-graining, and is significantly different from nano-scale materials science in which quantum size effect on electronic states is a key.

Magnetization in visible frequency range is a tough object and had been considered to be unrealistic due to the description in a famous textbook [3]. Recently, metallic structures of split-ring resonators (SRR) [4, 5], perforated metal-dielectric-metal layers [6], and short wire pairs [7] become candidates to be exceptions in visible range to the statement by Landau and Lifshitz [3]. Some of the results are based on experimental examination [6, 7], and revealed the resonant and anti-resonant behavior of permittivity and permeability [8]. As a result, the EM states in metamaterials turn out quite complicated and lossy.

A simple theoretical analysis presented a possibility of negative refractive index in a thin metal film [9] and the sub-diffraction-limited image was shown experimentally [10]. It is expected that near-EM-field enhancement is induced to compensate the loss at resonance with exploiting thin metallic layers. Another experimental result was reported which supports the enhancement by stratified thin metals [11]. Besides, it was very recently argued that negative refractive response appears in stratified stacks composed of metal-dielectric several layers [12]. Thus, the magnetic response in metallic thin films attracts great interest, connecting to optics with negative refraction.

In the present Communication, we specify stratified metal-dielectric metamaterials (SMDM) to examine ef-

fective magnetic response at visible frequencies. The schematic drawing of SMDM and the coordinate configuration are shown in Fig. 1. Since the structure is uniaxial, effective tensors of permittivity  $\varepsilon$  and permeability  $\mu$  are assumed to be diagonal and uniaxial:

$$\varepsilon = \begin{pmatrix} \varepsilon_x & 0 & 0 \\ 0 & \varepsilon_y & 0 \\ 0 & 0 & \varepsilon_z \end{pmatrix}, \quad \mu = \begin{pmatrix} \mu_x & 0 & 0 \\ 0 & \mu_y & 0 \\ 0 & 0 & \mu_z \end{pmatrix}. \quad (1)$$

The tensors are also assumed to describe local EM responses. The optical axis is set  $z$  axis, and then the two relations of  $\varepsilon_x = \varepsilon_y$  and  $\mu_x = \mu_y$  hold in Eq. (1). The periodicity is taken 75 nm. The thickness of metal (Ag) and dielectric ( $\text{MgF}_2$ ) are 15 and 60 nm, respectively. The thickness of silver layers was set to ensure using dielectric constant of bulk silver in literature [13].

We concentrate on bulk SMDM which is thick enough to eliminate transmission, and extract full components of  $\varepsilon$  and  $\mu$  tensors by two complex reflectivity method (TCRM). Although the method and numerical details were described already [14], we briefly survey the scheme in the following. Complex reflectivity  $r_s$  under  $s$  polar-

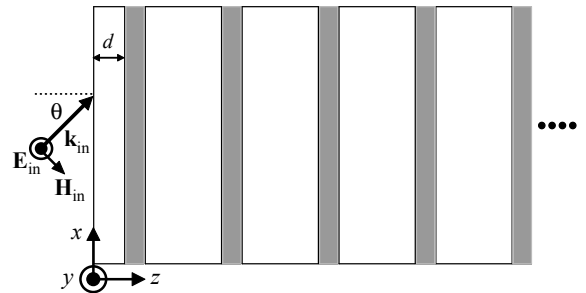


FIG. 1: Schematic drawing for structure of SMDM and coordinate configuration. Gray indicates metal (Ag) and white dielectric ( $\text{MgF}_2$ ). The thickness of surface layer is denoted by  $d$ . Incident light sheds on  $xy$  plane with  $s$  polarization (*i.e.*  $\mathbf{E}_{\text{in}} \parallel y$ ) and incident angle  $\theta$ . In this configuration, the two products of  $\varepsilon_y/\mu_x$  and  $\mu_x\mu_z$  are determined uniquely from two incident angles.

\*Electronic address: M.Iwanaga@osa.org

ization (that is,  $\mathbf{E}_{\text{in}} \parallel y$ ) in Fig. 1 satisfies at the interface:

$$\frac{\hat{k}_z(\theta)}{\mu_x} = \frac{n_0 \cos \theta}{\mu_0} \cdot \frac{1 - r_s(\theta)}{1 + r_s(\theta)}. \quad (2)$$

where  $\hat{k}_z(\theta)$  is the  $z$  component of refractive wavenumber vector normalized by wavenumber  $k_0$  in vacuum; in particular,  $\hat{k}_z(0)$  is refractive index along  $z$  axis. Besides,  $n_0$  and  $\mu_0$  denote the refractive index and permeability in vacuum. Equation of dispersion under  $s$  polarization is written as

$$\varepsilon_y = \frac{\hat{k}_z(\theta)^2}{\mu_x} + \frac{\hat{k}_x(\theta)^2}{\mu_z}, \quad (3)$$

where  $\hat{k}_x(\theta) = n_0 \sin \theta$  in the configuration of Fig. 1. Setting the right hand side of Eq. (2) to be  $f_s(\theta)$  and combining Eqs. (2) and (3), we obtain the next equation:

$$\frac{\varepsilon_y}{\mu_x} = f_s^2(\theta) + \frac{n_0^2 \sin^2 \theta}{\mu_x \mu_z}. \quad (4)$$

Two different angles ( $\theta_1 \neq \theta_2$ ) derive  $\sin \theta_1 \neq \sin \theta_2$ , and enable to evaluate  $\varepsilon_y/\mu_x$  and  $\mu_x \mu_z$  uniquely. By permutating the configuration  $(x, y, z) \rightarrow (y, z, x)$ , we can figure  $\varepsilon_z/\mu_y$  and  $\mu_y \mu_x$ . Since the relations of  $\varepsilon_x = \varepsilon_y$  and  $\mu_x = \mu_y$  are assumed for SMDM,  $\mu_x^2$  is evaluated; succeedingly, the rest components of  $\mu_z$ ,  $\varepsilon_x$ , and  $\varepsilon_z$  are uniquely obtained except for the sign. We set the sign of  $\mu_x$  to be  $\mu_x \approx 1$  at off-resonant energy of 1.5 eV and identify the sign without discontinuous jump as shown in Fig. 2. The precision in the computation for  $r_s$  ensures that the full components of tensors are determined within a few-percent numerical error.

Figure 2 presents the full components of (a)  $\varepsilon$  and (b)  $\mu$  tensors extracted by TCRM with the two angles of  $0^\circ$  and  $15^\circ$ . Other sets of two incident angles ( $0^\circ$  and  $\theta \neq 0^\circ$ ) result in the same spectra of  $\varepsilon_x$ ,  $\varepsilon_z$ , and  $\mu_x$  within a numerical error. In TCRM analysis using Eq. (4) and the angle pair  $(0^\circ, \theta)$ , it is easily found that  $\mu_z$  depends only on  $\theta$ ; therefore, we can extract  $\mu_z(\theta)$  at oblique angle. Thus, all the components of  $\varepsilon$  and  $\mu$  tensors are determined in a well-defined manner at visible frequencies in Fig. 2.

The  $\varepsilon_x$  component has typical dispersion of Drude metal (upper solid and dotted lines in Fig. 2(a): the real and imaginary parts of  $\varepsilon_x$ , respectively), and the effective plasma frequency  $\omega_{p,\text{eff}}$ , which is defined by  $\text{Re}(\varepsilon_x(\omega_{p,\text{eff}})) = 0$ , is located at  $\omega_{p,\text{eff}} = 2.6$  eV. On the other hand, the  $\varepsilon_z$  spectrum exhibits typical dielectric properties for the incident light of  $\mathbf{E}_{\text{in}} \parallel z$  (lower solid and dotted lines in Fig. 2(a): the real and imaginary parts of  $\varepsilon_z$ , respectively). Concerning permeability components,  $\mu_x$  is close to 1 at 1.5–3.5 eV (upper solid and dotted lines in Fig. 2(b): the real and imaginary parts of  $\mu_x$ , respectively), while  $\mu_z$  goes down to 0.57 at 2.6 eV and indicates strong diamagnetism (lower solid and dotted lines in Fig. 2(b): the real and imaginary parts of  $\mu_z$ , respectively). Refractive indexes along  $x$  and  $z$  axes are shown in Fig.

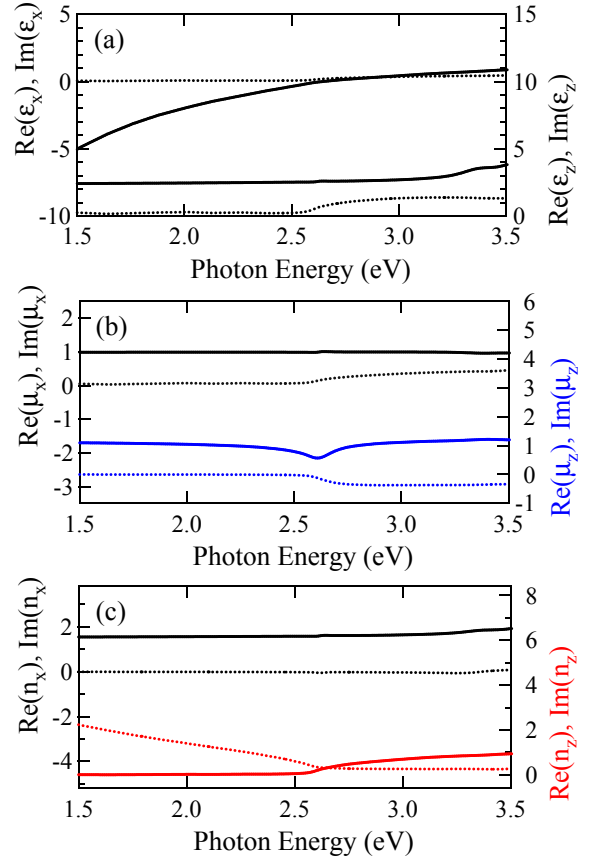


FIG. 2: Effective optical constants of SMDM, extracted with the two incident angles of  $0^\circ$  and  $15^\circ$ . (a): Effective permittivity. Upper solid line denotes  $\text{Re}(\varepsilon_x)$  and upper dotted line does  $\text{Im}(\varepsilon_x)$ . Lower two lines represent  $\varepsilon_z$  similarly. (b): Effective permeability. Lines indicate  $\mu_x$  and  $\mu_z$  with the notation similar to (a). (c): Effective refractive index along  $x$  and  $z$  axes. The real parts are shown with solid lines and the imaginary parts with dotted lines.

2(c); the upper solid and dotted lines respectively denote  $\text{Re}(n_x)$  and  $\text{Im}(n_x)$ , and the lower solid and dotted lines respectively stand for  $\text{Re}(n_z)$  and  $\text{Im}(n_z)$ . The imaginary parts of  $n_x$  and  $n_z$  are small above  $\omega_{p,\text{eff}}$ , and correspond to efficient EM-wave propagation.

In Fig. 3, we examine the validity of description by effective refractive index. The interface of vacuum and SMDM is set at  $z = 0$  and incident light of 2.65 eV illuminates on  $xy$  plane normally. Solid lines denote (a) electric and (b) magnetic fields of incident light in vacuum ( $z < 0$ ); they represent refractive components of electric and magnetic fields in SMDM ( $z > 0$ ). Dashed lines present the effective field profiles calculated by using  $n_z$  in Fig. 2(c) and reproduce the profiles in SMDM well. It is thus confirmed that the effective description works well in the visible range of interest.

As shown in Fig. 2, diamagnetic response is detected in  $\mu_z$ . This implies that magnetic induction  $B_z$  and magnetic field  $H_z$  behave in a different way. Figure 4 displays the image plot of (a)  $B_z$  and (b)  $H_z$  at 2.65 eV. Arrows

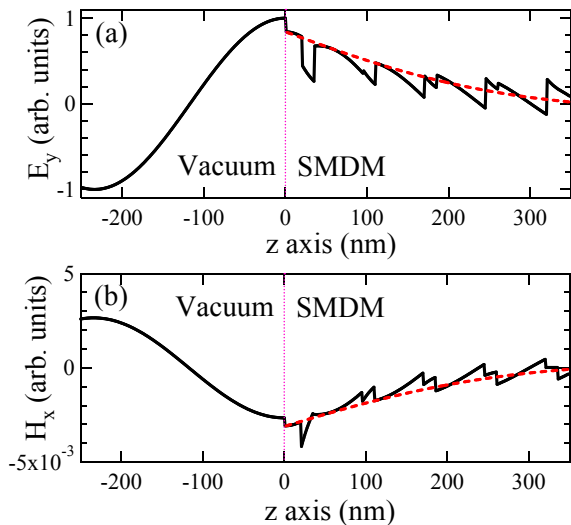


FIG. 3: Test for effective description. (a): Electric field is calculated at 2.65 eV under normal incidence on  $xy$  plane with  $s$  polarization. Solid line indicates forwardly propagating components, that is, incident and refractive components. Dashed line represents the effective electric field calculated by  $n_z$  in Fig. 2(c). Vertical dotted line indicates the interface. (b): Magnetic field, corresponding to (a).

denote the vectors at dotted points. In vacuum ( $z < 0$ ), the incident light travels with incident angle  $15^\circ$ , while in SMDM ( $z > 0$ ) both forward and backward components are displayed simultaneously because reflectance  $R$  is not small ( $R \sim 0.9$ ) and the backward components connected

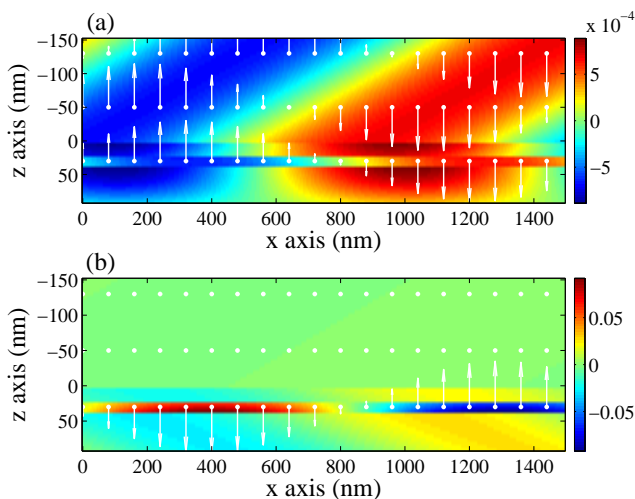


FIG. 4: Comparison of (a)  $B_z$  and (b)  $H_z$ . The region of vacuum ( $z < 0$ ) for simplicity shows incident light under oblique incidence of  $\theta = 15^\circ$ , and that of SMDM ( $z > 0$ ) contains both forwardly and backwardly propagating components. Arrows indicate the vectors at typical points (dots). In particular, the directions of  $B_z$  and  $H_z$  in metallic layer ( $20 < z < 35$  nm) are clearly opposite.

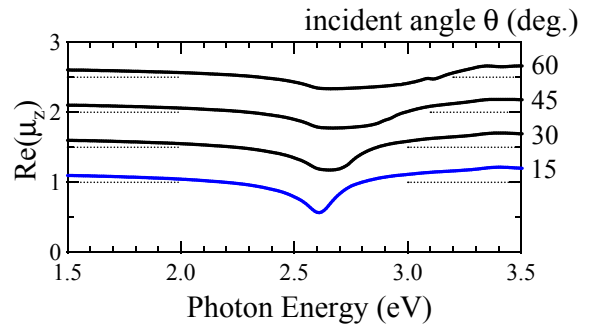


FIG. 5: Spatially dispersive behavior of  $\mu_z$  resonance. All the spectra are obtained by TCRM with the two angles of  $0^\circ$  and  $\theta (\neq 0^\circ)$ . However, as described in the text,  $\mu_z$  depends only on  $\theta$ . The spectrum at  $15^\circ$  is the same with that in Fig. 2(b). The spectra at  $\theta = 30^\circ, 45^\circ$ , and  $60^\circ$  are offset for visibility by 0.5, 1.0, and 1.5, respectively. Horizontal dotted lines indicate  $\text{Re}(\mu_z) = 1.0$  for each spectrum.

to inner multi-reflection is not negligible. When the EM fields are monochromatic plane waves and proportional to  $\exp(i\mathbf{k} \cdot \mathbf{r} - i\omega t)$ , the computation for  $B_z$  is carried out from one of Maxwell equations:

$$i\omega\mathbf{B} = i\mathbf{k} \times \mathbf{E}. \quad (5)$$

Magnetic field  $H_z$  is also calculated from

$$i\mathbf{k} \times \mathbf{H} = -i\omega\mathbf{D}. \quad (6)$$

Figure 4 obviously shows that the directions of  $B_z$  and  $H_z$  are opposite in metallic layer ( $20 < z < 35$  nm). Dielectric layers behave like paramagnetic materials. Besides, the  $H_z$  component in the metallic layer is far more intense than the  $H_z$  in vacuum and dielectric layers. In this way, the metallic layers act as if they are diamagnetic materials. The diamagnetic nature does not come from electronic spin states of silver but from superimposed magnetic field in mesoscopic structure of SMDM. The backward component is indeed responsible for the diamagnetic response. In this sense, the diamagnetic response is effectively induced by the structure in the metamaterial and is actually extracted by using effective optical constants. We can thus draw a concise picture by effective description.

Figure 5 shows the dependence of  $\mu_z$  on incident angle. Employing the two angles of  $0^\circ$  and  $\theta (\neq 0^\circ)$ , the extracted  $\mu_z$  depends only on  $\theta$ , as is easily verified from Eq. (4). The other components ( $\mu_x$ ,  $\varepsilon_x$ , and  $\varepsilon_z$ ) are almost independent of  $\theta$ . Therefore, the  $\mu_z$  spectra in Fig. 5 can be interpreted as the indication of spatial dispersion, that is,  $\mu_z = \mu_z(\mathbf{k})$  where  $\mathbf{k}$  is the wavenumber vector in SMDM. As is shown in Fig. 4, the effective diamagnetic response is generated in the mesoscopic structure of SMDM and moreover emerges at  $\omega_{p,\text{eff}}$ . Consequently, the effective diamagnetic response is regarded as magnetic component of collective excitation at  $\omega_{p,\text{eff}}$ . Note that  $\mu_z$  at off-resonance below 2.3 eV is almost indepen-

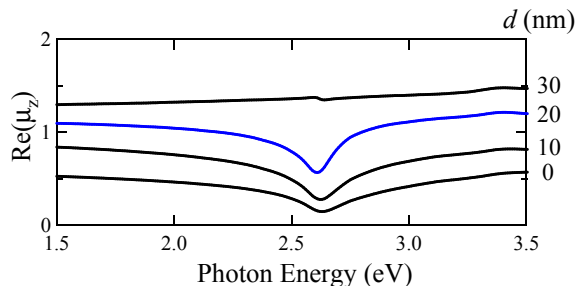


FIG. 6: Permeability  $\mu_z$  spectra of SMDM with various surface layers: the thickness  $d$  of surface layers from 0 to 30 nm. All the spectra are determined with the two incident angles of  $0^\circ$  and  $15^\circ$ , and are presented without vertical offset. The spectrum of  $d = 20$  nm in Fig. 5 is displayed again for comparison.

dent of  $\theta$  and the spatial dispersion is a resonant behavior.

Figure 6 displays the effect of surface layer on the effective  $\mu_z$ . Figures 2–5 are the results regarding the surface thickness  $d = 20$  nm; the spectra is shown again in Fig. 6. From bottom to top, the thickness  $d$  varies from 0 to 30 nm, respectively. SMDMs with  $d = 0$  and 10 nm show diamagnetic property in a wide frequency range. The increase of surface thickness  $d$  gradually cancels diamagnetic response and finally eliminate the diamagnetism at  $d = 30$  nm. Since the surface layer directly affects the phase of EM wave in SMDM, it is crucially significant how to set the surface layer in realizing the diamagnetism. Figure 6 is the explicit indication, which is consistent with the conclusion in a recent numerical study [15], showing that the interfaces play a vital role in photonic slabs of finite thickness, in extracting effective constants.

As is shown in Figs. 4 and 6, the effective diamagnetic response emerges at  $\omega_{p,\text{eff}}$ , comes from the stratified metallic layers, and is directly connected to the surface layer in SMDM. In other words, the diamagnetic resonance is induced in the mesoscopic structure including the surface layer. Indeed, as the  $\omega_{p,\text{eff}}$  shifts with varying the ratio of metal in the unitcell, the diamagnetic resonance follows the shift of  $\omega_{p,\text{eff}}$ . Furthermore, it is spatially dispersive as indicated in Fig. 5. Although there is not yet general theory to elucidate the relation of EM resonances with mesoscopic structures, the origin of the diamagnetic resonance is different from that of magnetic resonance in SRR, which has Lorentian frequency dispersion, and does not show spatial dispersion. The magnetic

resonance in SRR has an analogy to the resonance in LC circuit [5].

From computational and theoretical studies, it was reported that magnetism takes place in the systems composed of dielectric [16, 17] and metallic rods [18, 19], comes from the Mie resonances peculiar to the rods, and is spatially dispersive [17, 18]. There is another approach to analyze the media of metallic rods in view of nonlocal response [20]; strong spatial dispersion was shown even in the very long wavelength limit. Thus, several theoretical approaches have been proposed so far. In order to test them, it is probably necessary to extract, using the theories, effective optical constants in concrete systems, as is performed here.

We have focused on thick enough SMDM in this Communication. Of course, this system is not easily fabricated in reality. However, it is a good touchstone to examine how the effective optical responses emerge in periodic metal-dielectric systems. As long as the effective constants are valid for semi-infinite system, the system of finite thickness is probably described except for the interference effects associated with another surface. In the present analysis, there is no evidence to indicate negative refraction in SMDM, which was lately argued in finite systems [12]. If negative refraction took place in finitely thick SMDM, it should be due to an interference effect.

In conclusion, we have numerically extracted the full components of effective tensors of  $\varepsilon$  and  $\mu$  in SMDM by TCRM in a well-defined way, and clarified the effective diamagnetic resonance along the optical axis. The diamagnetism originates from the EM response in mesoscopic structure composed of stratified metals. The effective optical responses in metamaterials directly result from the mesoscopic structure including the surface layers. Moreover, it has been shown that the resonance is spatially dispersive. The diamagnetic nature of thin metals is experimentally feasible, and it is expected to open a new route to nonlinear optical processes using diamagnetic resonance.

### Acknowledgments

The author thanks T. Ishihara and S. G. Tikhodeev for stimulating discussion. This study was partially supported by Research Foundation for Opto-Science and Technology and by the Information Synergy Center, Tohoku University in numerical implementation.

- 
- [1] J. B. Pendry and D. R. Smith, *Phys. Today* **57**(6), 37 (2004).  
 [2] V. M. Shalaev, *Nature Photon.* **1**, 41 (2007).  
 [3] L. D. Landau and E. M. Lifshitz, *Electrodynamics of Continuous Media* (Pergamon, New York, 1984), 2nd ed.

- [4] A. Ishikawa, T. Tanaka, and S. Kawata, *Phys. Rev. Lett.* **95**, 237401 (2005).  
 [5] J. Zhou, T. Koschny, M. Kafesaki, E. N. Economou, J. B. Pendry, and C. M. Soukoulis, *Phys. Rev. Lett.* **95**, 223902 (2005).

- [6] G. Dolling, M. Wegener, C. M. Soukoulis, and S. Linden, *Opt. Lett.* **32**, 53 (2007).
- [7] H.-K. Yuan, U. K. Chettiar, W. Cai, A. V. Kildishev, A. Boltasseva, V. P. Drachev, and V. M. Shalaev, *Opt. Express* **15**, 1076 (2007).
- [8] T. Koschny, P. Markoš, D. R. Smith, and C. M. Soukoulis, *Phys. Rev. E* **68**, 065602(R) (2003); *ibid* **70**, 048603 (2004).
- [9] J. B. Pendry, *Phys. Rev. Lett.* **85**, 3966 (2000).
- [10] N. Fang, H. Lee, C. Sun, and X. Zhang, *Science* **305**, 534 (2005).
- [11] M. Scalora, M. J. Bloemer, A. S. Manka, S. D. Pethel, J. P. Dowling, and C. M. Bowden, *J. Appl. Phys.* **83**, 2377 (1998).
- [12] M. Scalora, G. D'Aguanno, N. Mattiucci, M. J. Bloemer, D. de Ceglia, M. Centini, C. Sibilia, N. Akozbek, M. G. Cappeddu, M. Fowler, et al., *Opt. Express* **15**, 508 (2007).
- [13] P. B. Johnson and R. W. Christy, *Phys. Rev. B* **6**, 4370 (1972).
- [14] M. Iwanaga, *Opt. Lett.* (to be published), posted as Doc. ID 78547.
- [15] T. Decoopman, G. Tayeb, S. Enoch, D. Maystre, and B. Gralak, *Phys. Rev. Lett.* **97**, 073905 (2006).
- [16] K. C. Huang, M. L. Povinelli, and J. D. Joannopoulos, *Appl. Phys. Lett.* **85**, 543 (2004).
- [17] D. Felbacq and G. Bouchitté, *Phys. Rev. Lett.* **94**, 183902 (2005).
- [18] D. Felbacq and G. Bouchitté, *Opt. Lett.* **30**, 1189 (2005).
- [19] X. Hu, C. T. Chan, J. Zi, M. Li, and K. M. Ho, *Phys. Rev. Lett.* **96**, 223901 (2006).
- [20] P. A. Belov, R. Marqués, S. I. Maslovski, I. S. Nefedov, M. Silveirinha, C. R. Simovski, and S. A. Tretyakov, *Phys. Rev. B* **67**, 113103 (2003).